

## CONFIRMING THE QUIESCENT GALAXY POPULATION OUT TO $z = 3$ : A STACKING ANALYSIS OF MID-, FAR-INFRARED AND RADIO DATA

ALLISON W. S. MAN<sup>1,2</sup>, THOMAS R. GREVE<sup>3</sup>, SUNE TOFT<sup>1</sup>, BENJAMIN MAGNELLI<sup>4</sup>, ALEXANDER KARIM<sup>4</sup>, OLIVIER ILBERT<sup>5</sup>,  
MARA SALVATO<sup>6</sup>, EMEIC LE FLOC'H<sup>7</sup>, FRANK BERTOLDI<sup>4</sup>, CAITLIN M. CASEY<sup>8</sup>, NICHOLAS LEE<sup>2</sup>, YANXIA LI<sup>2</sup>, FELIPE  
NAVARRETE<sup>4</sup>, KARTIK SHETH<sup>9</sup>, VERNESA SMOLČIĆ<sup>10</sup>, DAVID B. SANDERS<sup>2</sup>, EVA SCHINNERER<sup>11</sup>, AND ANDREW W. ZIRM<sup>1</sup>

*Submitted to ApJL*

### ABSTRACT

We present stringent constraints on the average mid-, far-infrared and radio emissions of  $\sim 14200$  quiescent galaxies (QGs), identified out to  $z = 3$  in the COSMOS field via their rest-frame NUV–r and r–J colors, and with stellar masses  $M_\star = 10^{9.8-12.2} M_\odot$ . Stacking in deep *Spitzer* (MIPS  $24\mu\text{m}$ ), *Herschel*<sup>†</sup> (PACS and SPIRE), and VLA (1.4 GHz) maps reveals extremely low dust-obscured star formation rates for QGs (SFR  $< 0.1-3 M_\odot\text{yr}^{-1}$  at  $z \leq 2$  and  $< 6-18 M_\odot\text{yr}^{-1}$  at  $z > 2$ ), consistent with the low unobscured SFRs ( $< 0.01-1.2 M_\odot\text{yr}^{-1}$ ) inferred from modeling their ultraviolet-to-near-infrared photometry. The average SFRs of QGs are  $> 10\times$  below those of star-forming galaxies (SFGs) within the  $M_\star$ - and  $z$ -ranges considered. The stacked 1.4 GHz signals (S/N  $> 5$ ) are, if attributed solely to star formation, in excess of the total (obscured plus unobscured) SFR limits, suggestive of a widespread presence of low-luminosity active galactic nuclei (AGN) among QGs. Our results reaffirm the existence of a significant population QGs out to  $z = 3$ , thus corroborating the need for powerful quenching mechanism(s) to terminate star formation in galaxies at earlier epochs.

*Subject headings:* galaxies: evolution — galaxies: high-redshift — galaxies: ISM — galaxies: star formation — galaxies: statistics — infrared: ISM

### 1. INTRODUCTION

Half of the most massive ( $M_\star \geq 10^{11} M_\odot$ ) galaxies at  $z \sim 1.5$  have evolved stellar populations and SFRs of only a few  $M_\odot\text{yr}^{-1}$  (e.g., [Ilbert et al. 2013](#), and references therein), suggesting that they have undergone a rapid build-up of stellar mass followed by an effective phase of star formation (SF) quenching, probably via AGN feedback (e.g., [Bower et al. 2006](#); [Croton et al. 2006](#)). If significant dust is present in these galaxies, however, it would imply that the SFRs, inferred from the rest-frame ultraviolet (UV), are severely underestimated, and that their stellar populations are in fact not old but simply reddened by the dust. Direct far-infrared

(FIR) measurements of the dust are therefore essential to unambiguously assess the level of obscured SF. A recent *Herschel* stacking analysis by [Viero et al. \(2013\)](#) found that massive QGs at  $z > 2$  have IR luminosities comparable to local ultra-luminous IR galaxies (ULIRGs,  $L_{\text{IR}} \geq 10^{12} L_\odot$ ), inconsistent with the quiescence inferred from the UV continua (e.g., [Ilbert et al. 2013](#)) as well as their low  $24\mu\text{m}$  stacked flux densities ([Fumagalli et al. 2013](#); [Utomo et al. 2014](#)). If QGs harbor significant dust-obscured SF, it would challenge the need for powerful quenching mechanisms.

Here, we analyse a sample of  $\sim 14200$  QGs with  $M_\star = 10^{9.8-12.2} M_\odot$  out to  $z = 3$ , selected over  $1.48\text{ deg}^2$  in the COSMOS field. Taking advantage of the available deep multi-wavelength data, we constrain their dust-obscured SFRs through stacking in *Spitzer* Multiband Imaging Photometer (MIPS), *Herschel* Photodetector Array Camera and Spectrometer (PACS; [Poglitsch et al. 2010](#)) and Spectral and Photometric Imaging Receiver (SPIRE; [Griffin et al. 2010](#)) maps. These are compared with stacks in deep Very Large Array (VLA) radio maps. We infer extremely low levels of dust-obscured SF ( $< [0.3, 3, 18] M_\odot\text{yr}^{-1}$  at  $z \sim [0.8, 1.7, 2.6]$ ), thus definitively confirming the quiescent nature of these galaxies.

Magnitudes are quoted in the AB system. We adopt a [Chabrier \(2003\)](#) initial mass function, and  $H_0 = 70\text{ km s}^{-1}\text{Mpc}^{-1}$ ,  $\Omega_M = 0.3$  and  $\Omega_\Lambda = 0.7$ .

### 2. DATA AND SAMPLE SELECTION

We select galaxies brighter than  $K_s = 24$  from the UltraVISTA survey ([McCracken et al. 2012](#)) that have  $M_\star \geq 10^{9.8} M_\odot$  and photometric redshifts  $z_{\text{phot}} = 0.1 - 3.0$ . Both  $M_\star$  and  $z_{\text{phot}}$  are from [Ilbert et al. \(2013\)](#), derived from spectral energy distribution (SED) fits to broadband UV-to-IRAC photometry ([Capak et al. 2007](#);

Electronic address: [allison@dark-cosmology.dk](mailto:allison@dark-cosmology.dk)

<sup>1</sup> Dark Cosmology Centre, Niels Bohr Institute, University of Copenhagen, Denmark

<sup>2</sup> Institute for Astronomy, 2680 Woodlawn Drive, University of Hawaii, Honolulu, HI 96822, USA

<sup>3</sup> Department of Physics and Astronomy, University College London, Gower Street, London WC1E 6BT, UK

<sup>4</sup> Argelander-Institut für Astronomie, Universität Bonn, Auf dem Hügel 71, D-53121 Bonn, Germany

<sup>5</sup> Aix Marseille Université, CNRS, Laboratoire d'Astrophysique de Marseille, UMR 7326, F-13388 Marseille, France

<sup>6</sup> Max-Planck-Institut für extraterrestrische Physik, Garching bei München, D-85741 Garching bei München, Germany

<sup>7</sup> Laboratoire AIM, CEA/DSM/IRFU, CNRS, Université Paris-Diderot, 91190 Gif, France

<sup>8</sup> Department of Physics and Astronomy, University of California, Irvine, CA 92697, USA

<sup>9</sup> National Radio Astronomy Observatory, 520 Edgemont Road, Charlottesville, VA 22903, USA

<sup>10</sup> Physics Department, University of Zagreb, Bijenička cesta 32, 10002 Zagreb, Croatia

<sup>11</sup> Max-Planck-Institut für Astronomie, Königstuhl 17, D-69117 Heidelberg, Germany

<sup>†</sup> *Herschel* is an ESA space observatory with science instruments provided by European-led Principal Investigator consortia and with important participation from NASA.

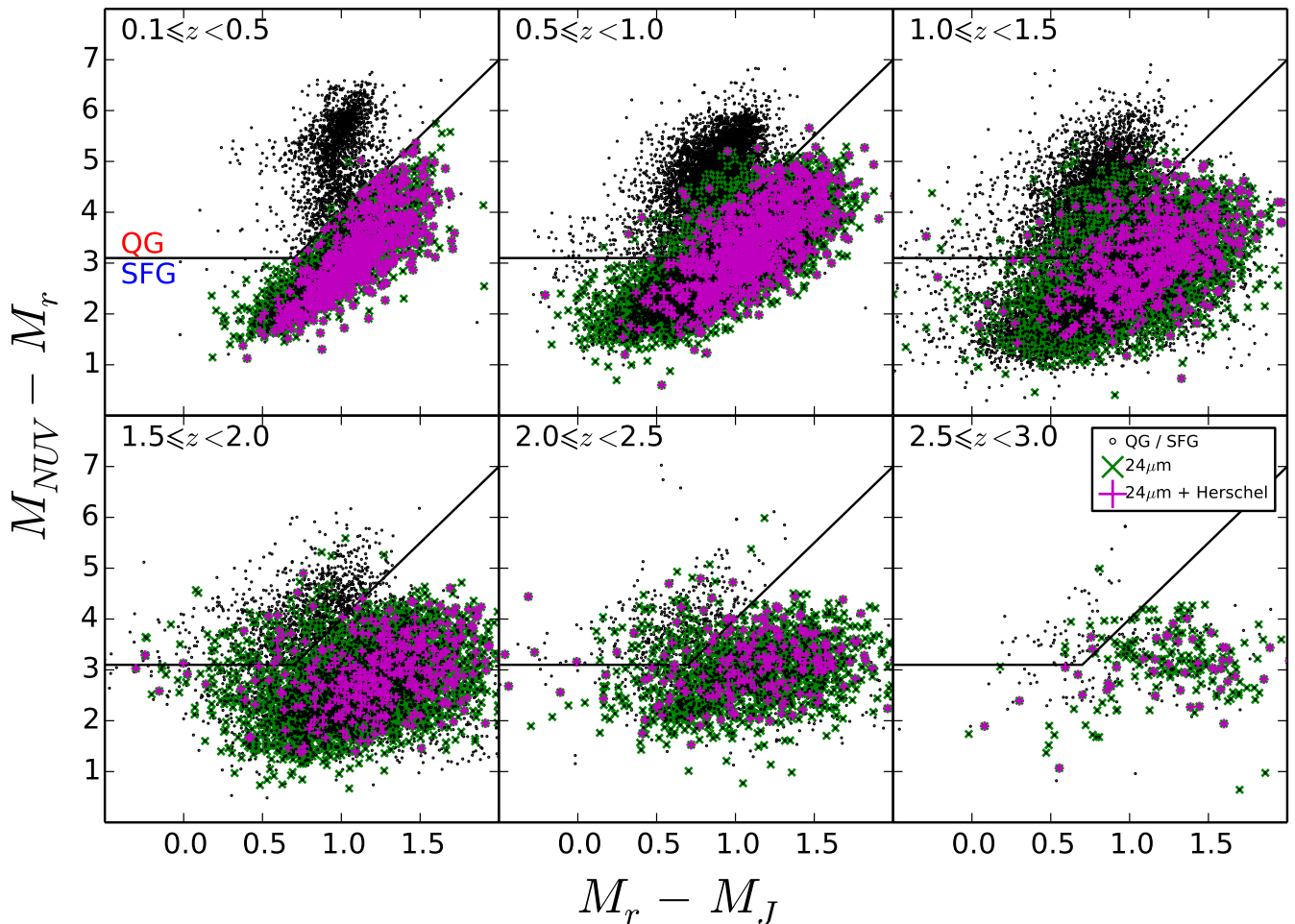


FIG. 1.— Rest-frame NUV- $r$  and  $r$ - $J$  colors for galaxies above the mass-completeness limits (small black circles) from the UltraVISTA survey. QGs are defined as having  $M_{\text{NUV}} - M_r > 3(M_r - M_J) + 1$  and  $M_{\text{NUV}} - M_r > 3.1$ . The QGs/SFGs classification boundary is marked by black solid lines. Galaxies with  $\text{SFR}_{24} > 20 M_{\odot} \text{yr}^{-1}$  (green crosses) and *Herschel* detections (magenta pluses) are indicated (fractions of the total QG sample are listed in Table 1).

Scoville et al. 2007). A small number of AGN, identified via their emission in X-rays (Brusa et al. 2010; Civano et al. 2012), IRAC bands (Donley et al. 2012), or the radio (Schinnerer et al. 2007, 2010), are removed to minimise the effects of erroneous SED fits and thus inaccurate  $z_{\text{phot}}$  and  $M_{\star}$ . Including the AGN in the analysis does not change the stacked flux densities (within the uncertainties) nor the conclusions of this Letter.

Each galaxy is classified as a QG or a SFG based on its rest-frame NUV- $r$  and  $r$ - $J$  colors (Figure 1). NUV- $r$  is a measure of the amount of UV light from young stars (i.e., recent SF) relative to the red optical light from evolved stellar populations, while  $r$ - $J$  constrains the degree of dust attenuation in the red part of the spectrum. The QGs are divided into six bins of  $z_{\text{phot}}$ , each of which is split into four  $M_{\star}$ -bins (see Table 2); however, only  $M_{\star}$ -bins which are  $> 90\%$  mass-complete (according to the limits presented in Ilbert et al. 2013) are included.

To weed out dusty galaxies erroneously classified as QGs, we cross-correlate our sample with the MIPS  $24 \mu\text{m}$  catalog of Le Floch et al. (2009) with a radius of  $2''$ . A redshift-dependent  $24 \mu\text{m}$  flux density ( $S_{24}$ ) cut-off is then applied to remove QGs with dust-obscured SFRs  $> 20 M_{\odot} \text{yr}^{-1}$  (as inferred from their  $S_{24}$  — see Section 4.2).

The fraction ( $f_{\text{QG},24}$ ) of QGs with  $24 \mu\text{m}$ -inferred SFRs  $> 20 M_{\odot} \text{yr}^{-1}$  increases with redshift and peaks at 13–19% for the most massive  $z \gtrsim 2$  QGs (see Table 1). This suggests a higher fraction of misclassified QGs at  $z \gtrsim 2$ , which is unsurprising given their faintness ( $i \gtrsim 25$ ). Overall, however, the fractions are reassuringly small. A similar conclusion is reached from the fraction ( $f_{\text{QG,H}}$ ) of *Herschel* detected QGs ( $< 6\%$ ), determined using the catalog of Lee et al. (2013) in which the  $24 \mu\text{m}$  sources are cross-identified to the *Herschel* detections (i.e.,  $\text{S/N} \geq 5$  in at least two PACS or SPIRE bands). This population of dusty galaxies having quiescent NUV- $r$  and  $r$ - $J$  colors could either be SFGs with strong attenuation, or galaxies containing evolved stellar populations and undergoing rejuvenation of SF (Lemaux et al. 2013). The robust *Herschel* detections in the QG region tend to lie close to the QG/SFG classification boundary at least out to  $z = 1.5$  (Figure 1), perhaps indicative of their post-starburst nature (Hayward et al. 2014).

For the stacking analysis (Section 3) we use the aforementioned MIPS  $24 \mu\text{m}$  imaging ( $\text{FWHM} \simeq 6''$ ) from Sanders et al. (2007), while the *Herschel* PACS and SPIRE maps are from the PACS Evolutionary Probe survey (PEP; Lutz et al. 2011) and the *Herschel* Multi-

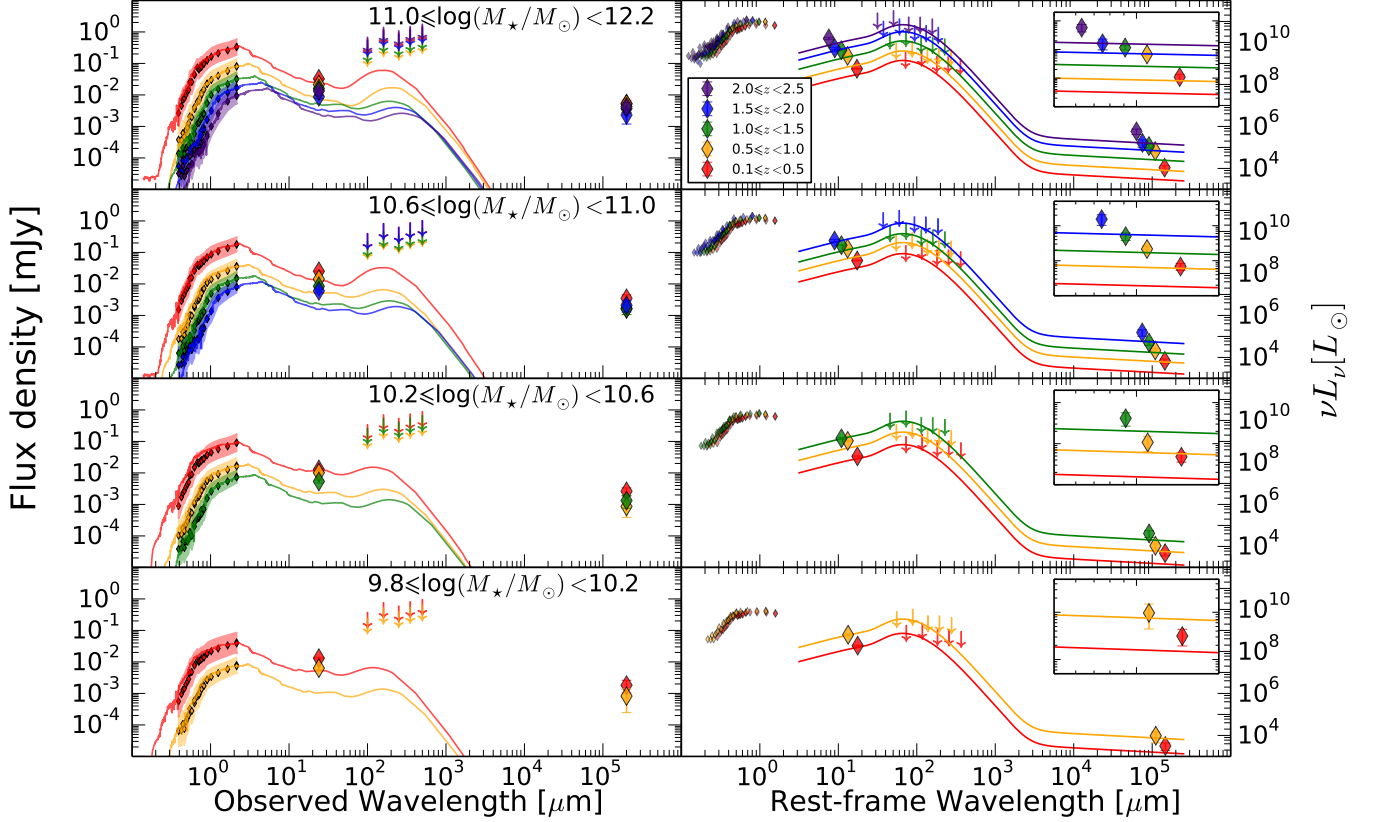


FIG. 2.— Panchromatic SEDs of QGs in four  $M_*$ -bins (rows) and six  $z$ -bins (colors) in observed (left) and rest-frame (right) frames. The median UV-to-near-IR photometry is plotted and shaded with its standard deviations. The longer wavelength data represent our stacking results. *Left*: At  $z > 0.5$  the observed  $S_{24}$  are higher than that expected from pure stellar emissions of elliptical galaxy models of Bruzual & Charlot 2003 (matched to the median stellar ages from SED fits and scaled to  $K$ -band magnitudes). *Right*: The FIR black-body models (Casey 2012) fitted to the *Herschel* upper limits (assuming  $T_{\text{dust}} = 30$  K) are co-joined with a radio power-law ( $\alpha = -0.8$ ) and plotted as lines, following the radio-FIR correlation presented in Ivison et al. (2010) with shallow redshift evolution. The templates are not fitted to the radio data. Shown in the insets, the observed  $S_{\text{radio}}$  is higher than expected from SF. The  $24\ \mu\text{m}$  and radio excesses suggest contributions from low-luminosity AGN.

tiered Extragalactic Survey (HerMES; Oliver et al. 2012), respectively. The PACS maps reach depths of 5 and  $10.3\ \text{mJy beam}^{-1}$  ( $3\sigma$ ) at 100 and  $160\ \mu\text{m}$ , respectively (FWHM  $\simeq 6.8''$  and  $11''$ ), and SPIRE 250, 350, and  $500\ \mu\text{m}$  depths are 8, 11, and  $13\ \text{mJy beam}^{-1}$  ( $3\sigma$ ), respectively (FWHM  $\simeq 18.2''$ ,  $24.9''$ , and  $36.3''$ ). For the radio stacking we use the 1.4 GHz VLA-COSMOS large survey (Schinnerer et al. 2007, 2010), which reaches a root-mean-square noise (rms) of  $15\ \mu\text{Jy beam}^{-1}$  at an angular resolution of  $\sim 1.5''$  (FWHM).

### 3. STACKING

Our *Herschel* maps are characterised by a high level of source confusion which, if unaccounted for, will bias a stacked signal (Marsden et al. 2009; Béthermin et al. 2010; Kurczynski & Gawiser 2010; Viero et al. 2013). Here, we use a global deblending technique similar to that of Kurczynski & Gawiser (2010) but generalised to deblend multiple galaxy samples simultaneously, which in our case totaled 87 samples (separated by their SFG/QG classifications,  $z$ - and  $M_*$ -bins, and  $\text{SFR}_{24}$  threshold).

Source confusion is not an issue for our radio maps due to the high angular resolution, and the stacked signal of a given sample was determined from the median combination of the galaxy postage stamps belonging to the

sample. The MIPS  $24\ \mu\text{m}$  stacks were determined in a similar way, despite the larger beam size. To ensure that our  $24\ \mu\text{m}$  median stacks were not biased, we stacked samples of SFGs using the global deblending technique and found excellent agreement with the median results. The  $24\ \mu\text{m}$  flux densities were measured on the stacked images using an aperture radius of  $3.5''$  with aperture corrections applied following the MIPS handbook. For the radio fluxes we adopted the central pixel values. In both cases the errors were estimated from the rms of the background in the stacked images.

### 4. RESULTS

#### 4.1. Panchromatic UV-to-radio SEDs of QGs

The stacked MIPS  $24\ \mu\text{m}$ , *Herschel*, and radio flux densities of the  $z$ - and  $M_*$ -bins of QGs are listed in Table 2. None of the QG samples are significantly detected (i.e.,  $\text{S/N} > 3$ ) in any of the *Herschel* stacks. The most massive ( $M_* \geq 10^{10.6} M_\odot$ ) QGs are detected at all redshifts out to  $z = 3$  in the  $24\ \mu\text{m}$  stacks ( $\text{S/N} \sim 5\text{--}26$ ) and out to  $z = 1.5$  in the radio stacks ( $\text{S/N} \sim 4\text{--}10$ ). The intermediate-mass QGs ( $M_* < 10^{10.6} M_\odot$ ) are detected at  $24\ \mu\text{m}$  ( $\text{S/N} \sim 5\text{--}20$ ) but not in the radio ( $\text{S/N} \leq 3$ ) in all relevant (i.e., mass-complete) redshift bins. As expected,  $S_{24}$  and  $S_{\text{radio}}$  decrease with  $z$  (cosmic dimming) and increase with  $M_*$ .

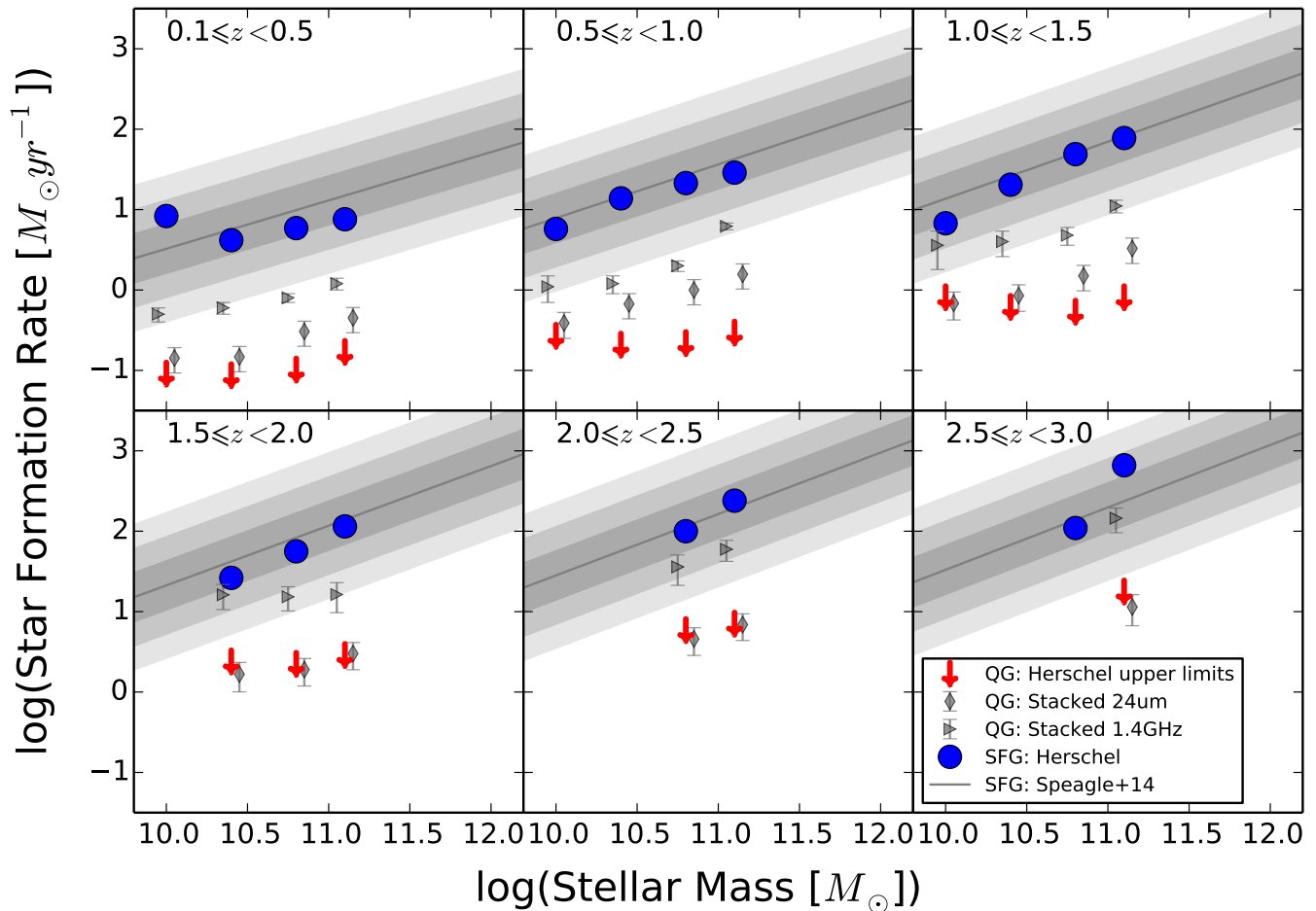


FIG. 3.— SFRs inferred from stacking as a function of  $M_*$  and  $z$ . Blue circles and red downward arrows represent the SFRs from global deblending and stacking in *Herschel* for SFGs and QGs respectively, with the latter ones representing  $3\sigma$  upper limits for QGs since they are consistent with no detection. Assuming the  $24\mu\text{m}$  and radio emissions originate from SF only, we plot the inferred SFRs as gray diamonds and triangles.  $\text{SFR}_{\text{radio}}$ , as well as  $\text{SFR}_{24}$  at  $z < 1.5$ , show clear offsets from  $\text{SFR}_H$  for QGs, therefore part of the radio emission in QGs likely arises from low-luminosity AGN. The  $\text{SFR}-M_*$  measured in a recent compilation (Speagle et al. 2014) is plotted as gray lines, and the  $1-3 \times$  observed dispersion ( $\sigma_{\text{SFR}}=0.3$ ) are shown as dark-to-light shades. QGs have SFRs at least  $\gtrsim 1$  dex below those of SFGs out to  $z \sim 3$ .

Figure 2 summarises our constraints on the SEDs of QGs at mid-, far-IR, and radio wavelengths along with the median UV-to-near-IR SEDs. Note, the *Herschel* non-detections are shown as  $3\sigma$  upper limits (i.e.  $3\sigma_{\text{map}}/\sqrt{N_{\text{stack}}}$ , where  $\sigma_{\text{map}}$  is the map rms noise and  $N_{\text{stack}}$  the number of galaxies in the stack). For comparison we show the SED template of a dust-free elliptical galaxy (Bruzual & Charlot 2003) scaled to match the UV-to-near-IR median photometry of the QGs (Figure 2, left). The model, which represents pure stellar emission, is insufficient to fully account for the stacked  $24\mu\text{m}$  flux densities. If we instead fit a modified black-body law (see details in Section 4.2) to the *Herschel* limits, add radio emission (a power-law with slope  $\alpha = -0.8$ ) such that the radio-FIR correlation (Ivison et al. 2010) is fulfilled, we still fall short of the stacked  $1.4\text{GHz}$  fluxes (Figure 2, right panels). The implications of this excess emission at  $24\mu\text{m}$  and  $1.4\text{GHz}$  are discussed in Section 4.3.

#### 4.2. Where do QGs lie relative to the SFGs on the $\text{SFR}-M_*$ relation?

The mid-, far-IR and radio stacks each provide an independent measurement of the dust-obscured SFRs in our

QGs. Firstly, we estimate the 8 to  $1000\mu\text{m}$  rest-frame IR luminosity ( $L_{\text{IR}}$ ) from  $S_{24}$  using the calibration by Rujopakarn et al. (2013), including the 0.13 dex scatter of the calibration in the error budget. Independent  $L_{\text{IR}}$  upper limits are then obtained by redshifting and scaling a modified black-body model to the *Herschel*  $3\sigma$  upper limits using the IDL code of Casey (2012). We use an optically thick, modified black-body law with a fixed dust temperature ( $T_{\text{dust}} = 30\text{K}$ ) and emissivity 1.5. Note that  $L_{\text{IR}}$  is insensitive to  $T_{\text{dust}}$ , as it only varies by less than a factor of two if we assume  $T_{\text{dust}} = 15\text{K}$  or  $50\text{K}$  instead. For each of our QG samples,  $L_{\text{IR}}$  is estimated in the above manner using the median  $z_{\text{phot}}$  (listed in Table 2), and subsequently converted into an obscured SFR using the  $L_{\text{IR}}$ -SFR calibration by Kennicutt (1998) adjusted to the IMF used in this work. Assuming that all the radio emission originates from SF, and a radio spectral index  $\alpha = -0.8$ , rest-frame  $1.4\text{GHz}$  luminosities ( $L_{1.4\text{GHz}}$ ) are derived from the radio stacks and subsequently converted to  $\text{SFR}_{\text{radio}}$  using the  $L_{1.4\text{GHz}}$ -SFR calibration by Bell (2003).

The *Herschel*  $L_{\text{IR}}$  upper limits and the (specific) SFRs for QGs as a function of  $M_*$  and  $z$  are listed in Table 2.



TABLE 1  
*Spitzer* 24  $\mu\text{m}$  AND *Herschel* DETECTED FRACTIONS FOR QGS

Redshift	$\log(M_\star/M_\odot)$			
	11 – 12.2	10.6 – 11	10.2 – 10.6	9.8 – 10.2
	$f_{\text{QG},24}$ ( $f_{\text{QG,H}}$ )	$f_{\text{QG},24}$ ( $f_{\text{QG,H}}$ )	$f_{\text{QG},24}$ ( $f_{\text{QG,H}}$ )	$f_{\text{QG},24}$ ( $f_{\text{QG,H}}$ )
0.1 – 0.5	0% (0%)	0.4% (0.2%)	0% (0%)	0.2% (0%)
0.5 – 1.0	4.6% (1.4%)	4.0% (1.0%)	2.2% (0.3%)	0.4% (0.1%)
1.0 – 1.5	9.9% (2.4%)	5.3% (1.0%)	2.4% (0%)	0.6% (0%)
1.5 – 2.0	8.8% (1.5%)	9.0% (1.4%)	7.5% (1.0%)	...
2.0 – 2.5	19.4% (6.0%)	17.4% (2.5%)	...	...
2.5 – 3.0	13.3% (2.7%)	...	...	...

NOTE. —  $f_{\text{QG},24}$  is the fraction of QGs (classified by their NUV–r and r–J colors) with 24  $\mu\text{m}$ -inferred SFRs  $> 20 M_\odot \text{yr}^{-1}$ .  $f_{\text{QG,H}}$  is the fraction of QGs fulfilling the above 24  $\mu\text{m}$  criterion that are also detected in at least two *Herschel* PACS+SPIRE bands ( $S/N \geq 5$ ).

The *Herschel* upper limits put stringent constraints on the dust-obscured SFR:  $< 1 M_\odot \text{yr}^{-1}$  at  $z < 1.5$  and at most  $< 18 M_\odot \text{yr}^{-1}$ , i.e.,  $\text{sSFR} \leq 10^{-(10-12)} \text{yr}^{-1}$ , across all  $z$  and  $M_\star$  bins. These limits are consistent with the quiescence inferred from the unobscured SFR from UV-to-IRAC SED fits ( $0.01\text{--}1.2 M_\odot \text{yr}^{-1}$ , see Table 2). QGs form stars at a very modest rate ( $> 10\times$  lower than SFGs, Figure 3). As a consistency check, we find that the stacked *Herschel* flux densities of SFGs obtained from global deblending and stacking (Kurczynski & Gawiser 2010) are in good agreement with those from median combination, and we recover the SFR- $M_\star$  sequence found in a recent compilation of similar measurements (Speagle et al. 2014, Figure 3).

#### 4.3. Do QGs host AGN?

$\text{SFR}_{24}$  are consistent with  $\text{SFR}_H$ , except at  $z < 1.5$  in which  $\text{SFR}_{24}$  is higher than  $\text{SFR}_H$  (by as much as  $5\times$ ), as shown in Figure 3. This discrepancy could be explained by the following factors not related to recent SF: (1) The Rayleigh-Jeans tail of the stellar photospheric emission, which is dominated by red giants; (2) Circumstellar dust envelopes of asymptotic giant branch (AGB) stars (Knapp et al. 1992; Piovani et al. 2003); (3) Interstellar (cirrus) dust heated by evolved stellar populations (e.g., Bendo et al. 2012); (4) Polycyclic aromatic hydrocarbon emission associated with (2) and (3) (Kennicutt 1998; Bendo et al. 2008); (5) Warm dust heated by the obscured AGN (Daddi et al. 2007). The first four factors are viable for galaxies with intermediate-old stellar populations ( $> 1 \text{ Gyr}$ , Salim et al. 2009). The elliptical galaxy template from stellar population synthesis models (Bruzual & Charlot 2003), which accounts for only (1) and to some extent (2), cannot fully reproduce the observed  $S_{24}$  at least for  $z > 0.5$  (Figure 2, left). This suggests that AGN and/or dust heating from evolved stellar populations are likely responsible for the low levels of  $L_{\text{IR}}$  of QGs (Salim et al. 2009; Bendo et al. 2012; Fumagalli et al. 2013; Utomo et al. 2014). The relative contribution of the above factors depends heavily on the evolution models of AGB stars, dust grain models and interstellar radiation strength, which are actively debated and beyond the scope of this Letter. While we cannot discern the relative contributions of dust heating from these factors using the data in hand, we note that the  $\text{SFR}_{24}$  are likely upper limits if non-SF processes contribute significantly to  $S_{24}$ .

It is interesting that  $\text{SFR}_{\text{radio}}$  is systematically higher than SFR inferred from 24  $\mu\text{m}$  and *Herschel* as well as UV-to-IRAC SED fits, up to two orders of magnitude in the most extreme case. Compared to the total (obscured + unobscured) SFR inferred from other indicators (*Herschel*, MIPS, UV-to-IRAC SED fitting), the median  $S_{\text{radio}}$  are inconsistent with originating from SF alone. This is reflected in the low radio index ( $q_{24} \equiv \log(S_{24}/S_{\text{radio}})$ ) listed in Table 2 compared to SFGs with typical values of 1.5 – 3 (e.g., Ivison et al. 2010).  $L_{1.4 \text{ GHz}}$  [W  $\text{Hz}^{-1}$ ] increases with redshift from  $10^{21.5}$  at  $z \sim 0.4$  to  $10^{23.7}$  at  $z \sim 2.6$  for the most massive QGs, where the radio excess is the most prominent (see Figure 2 right panel insets). Based on the FIR-radio correlation presented in Ivison et al. (2010) and including the radio-detected QGs in the stack, we estimate that 20-90% of  $L_{1.4 \text{ GHz}}$  arises from non-SF processes. This fraction is significantly higher for more massive QGs as shown in Figure 2, although we note that if we adopt a more conservative *Herschel* upper limit for the non-detection, the fraction will be lower. Our results indicate that low-luminosity radio AGN may be widespread among massive QGs, echoing the reciprocity that massive QGs are the preferential hosts for low-luminosity radio AGNs (e.g., Smolčić et al. 2009). However, it is not straightforward to use the median stacked radio luminosity to constrain the heating rate of radio-AGN feedback, without prior assumption of the duty cycle which is not well quantified.

## 5. DISCUSSION

We reject the null hypothesis that the red colors of QGs are due to strong obscured SF, based on a deep FIR stacking analysis. QGs have truly low SFRs and evolved stellar populations, as expected from their low unobscured SFRs measured from the UV continua. The average sSFRs of QGs are at least 1 dex lower than those of SFGs out to  $z = 3$ . The stacked 24  $\mu\text{m}$  and radio emissions cannot be completely accounted for by low levels of dust-obscured SFR nor stellar emissions, suggesting that low-luminosity AGN may be present in QGs.

Comparing with Fumagalli et al. (2013), who performed 24  $\mu\text{m}$  stacking on 309 QGs with  $M_\star \geq 10^{10.3} M_\odot$ , our  $S_{24}$  are slightly higher ( $5\text{--}26 \mu\text{Jy}$  vs  $2\text{--}3 \mu\text{Jy}$ ). Their sample is drawn from a smaller survey area equivalent to 11% of the UltraVISTA field, and therefore the discrepancy is likely explained by the fact that their

sample is dominated by lower mass galaxies, which have lower  $S_{24}$ . Nevertheless, we arrive at similar conclusions — QGs do not host strong obscured SF, and dust heating by evolved stellar populations may be significant at the low levels of  $L_{\text{IR}}$  observed. Our results indicate that  $z \gtrsim 2$  QGs have average  $L_{\text{IR}} \leq 10^{11.2} L_{\odot}$ , i.e.,  $\geq 0.8$  dex below the ULIRG threshold. When we repeat our stacking analysis including QGs detected at  $24\mu\text{m}$  following the definition of Viero et al. (2013), we obtain higher stacked mid- and far-IR emission, in broad agreement with their results. As QGs have higher  $24\mu\text{m}$  and *Herschel* detection fractions at  $z \gtrsim 2$  (up to 19% and 6%, respectively, see Table 1 and Section 2), the inclusion of the quoted fractions of  $L_{\text{IR}} > 10^{13} L_{\odot}$  sources boosts the stacked FIR emission of massive QGs at  $z \gtrsim 2$  to be comparable to ULIRGs.

We reaffirm that a population of truly quiescent galaxies is already in place by  $z = 3$ . This corroborates the need for powerful quenching mechanisms to terminate star formation in galaxies. While environmental quenching may be dominant for intermediate-mass QGs (Peng et al. 2010), stacking analyses at radio (this work) and X-ray (Olsen et al. 2013) wavelengths reveal that massive QGs harbor low-luminosity AGN. AGN provide a viable mechanism for quenching SF in galaxies, as supported by the enhanced AGN fraction among transitory objects between SFGs and QGs (e.g., Barro et al. 2014). After galaxies are quenched, the AGN may then proceed to “maintenance mode” suppressing further SF through

a feedback cycle (Schawinski et al. 2009; Best & Heckman 2012). With upcoming surveys it will be possible to conduct a complete census of AGN to sample the entire feedback duty cycle and constrain their energetics, in order to quantify their role in quenching star formation in galaxies.

We thank the COSMOS, UltraVISTA, PEP, and HERMES collaborations for providing the data used here. Dark Cosmology Centre is funded by DNRF. AM thanks Anna Gallazzi, Mark Sargent, Ryan Quadri, Brian Lemaux, and Julie Wardlow for helpful discussions. TRG acknowledges support from an STFC Advanced Fellowship. Support for BM was provided by the DFG priority program 1573 “The physics of the interstellar medium”. AK acknowledges support by the Collaborative Research Council 956, sub-project A1, funded by the Deutsche Forschungsgemeinschaft (DFG). CMC acknowledges support from a McCue Fellowship through the University of California, Irvine’s Center for Cosmology. VS is funded by the European Union’s Seventh Framework program (grant agreement 337595). Based on data products from observations made with ESO Telescopes at the La Silla Paranal Observatory under ESO programme ID 179.A-2005 and on data products produced by TERAPIX and the Cambridge Astronomy Survey Unit on behalf of the UltraVISTA consortium.

## REFERENCES

- Barro, G., et al. 2014, *ApJ*, 791, 52 [5]  
 Bell, E. F. 2003, *ApJ*, 586, 794 [4.2]  
 Bendo, G. J., et al. 2008, *MNRAS*, 389, 629 [4.3]  
 —. 2012, *MNRAS*, 419, 1833 [4.3]  
 Best, P. N., & Heckman, T. M. 2012, *MNRAS*, 421, 1569 [5]  
 Béthermin, M., Dole, H., Beelen, A., & Aussel, H. 2010, *A&A*, 512, A78 [3]  
 Bower, R. G., Benson, A. J., Malbon, R., Helly, J. C., Frenk, C. S., Baugh, C. M., Cole, S., & Lacey, C. G. 2006, *MNRAS*, 370, 645 [1]  
 Brusa, M., et al. 2010, *ApJ*, 716, 348 [2]  
 Bruzual, G., & Charlot, S. 2003, *MNRAS*, 344, 1000 [2, 4.1, 4.3]  
 Capak, P., et al. 2007, *ApJS*, 172, 99 [2]  
 Casey, C. M. 2012, *MNRAS*, 425, 3094 [2, 4.2]  
 Chabrier, G. 2003, *PASP*, 115, 763 [1]  
 Civano, F., et al. 2012, *ApJS*, 201, 30 [2]  
 Croton, D. J., et al. 2006, *MNRAS*, 365, 11 [1]  
 Daddi, E., et al. 2007, *ApJ*, 670, 173 [4.3]  
 Donley, J. L., et al. 2012, *ApJ*, 748, 142 [2]  
 Fumagalli, M., et al. 2013, *ArXiv e-prints* [1, 4.3, 5]  
 Griffin, M. J., et al. 2010, *A&A*, 518, L3 [1]  
 Hayward, C. C., et al. 2014, *MNRAS*, 445, 1598 [2]  
 Ilbert, O., et al. 2013, *A&A*, 556, A55 [1, 2]  
 Ivison, R. J., et al. 2010, *A&A*, 518, L31 [2, 4.1, 4.3]  
 Kennicutt, Jr., R. C. 1998, *ARA&A*, 36, 189 [4.2, 4.3]  
 Knapp, G. R., Gunn, J. E., & Wynn-Williams, C. G. 1992, *ApJ*, 399, 76 [4.3]  
 Kurczynski, P., & Gawiser, E. 2010, *AJ*, 139, 1592 [3, 4.2]  
 Le Floch, E., et al. 2009, *ApJ*, 703, 222 [2]  
 Lee, N., et al. 2013, *ApJ*, 778, 131 [2]  
 Lemaux, B. C., et al. 2013, *ArXiv e-prints* [2]  
 Lutz, D., et al. 2011, *A&A*, 532, A90 [2]  
 Marsden, G., et al. 2009, *ApJ*, 707, 1729 [3]  
 McCracken, H. J., et al. 2012, *A&A*, 544, A156 [2]  
 Oliver, S. J., et al. 2012, *MNRAS*, 424, 1614 [2]  
 Olsen, K. P., Rasmussen, J., Toft, S., & Zirm, A. W. 2013, *ApJ*, 764, 4 [5]  
 Peng, Y.-j., et al. 2010, *ApJ*, 721, 193 [5]  
 Piovan, L., Tantaló, R., & Chiosi, C. 2003, *A&A*, 408, 559 [4.3]  
 Poglitsch, A., et al. 2010, *A&A*, 518, L2 [1]  
 Rujopakarn, W., Rieke, G. H., Weiner, B. J., Pérez-González, P., Rex, M., Walth, G. L., & Kartaltepe, J. S. 2013, *ApJ*, 767, 73 [4.2]  
 Salim, S., et al. 2009, *ApJ*, 700, 161 [4.3]  
 Sanders, D. B., et al. 2007, *ApJS*, 172, 86 [2]  
 Schawinski, K., et al. 2009, *ApJ*, 690, 1672 [5]  
 Schinnerer, E., et al. 2007, *ApJS*, 172, 46 [2]  
 —. 2010, *ApJS*, 188, 384 [2]  
 Scoville, N., et al. 2007, *ApJS*, 172, 1 [2]  
 Smolčić, V., et al. 2009, *ApJ*, 696, 24 [4.3]  
 Speagle, J. S., Steinhardt, C. L., Capak, P. L., & Silverman, J. D. 2014, *ApJS*, 214, 15 [3, 4.2]  
 Utomo, D., Kriek, M., Labbé, I., Conroy, C., & Fumagalli, M. 2014, *ApJ*, 783, L30 [1, 4.3]  
 Viero, M. P., et al. 2013, *ApJ*, 779, 32 [1, 3, 5]

TABLE 2  
STACKED FLUX DENSITIES OF *Spitzer*/MIPS 24  $\mu\text{m}$ , *Herschel* (PACS+SPIRE), AND VLA 1.4 GHz AND THE INFERRED SFRs FOR QGs

Redshift	$\overline{z_{\text{phot}}}$	$N_{\text{stack}}$	$S_{24\mu\text{m}}$ [ $\mu\text{Jy}$ ]	$S_{100\mu\text{m}}$ [mJy]	$S_{160\mu\text{m}}$ [mJy]	$S_{250\mu\text{m}}$ [mJy]	$S_{350\mu\text{m}}$ [mJy]	$S_{500\mu\text{m}}$ [mJy]	$S_{\text{radio}}$ [ $\mu\text{Jy}$ ]	$\text{SFR}_{\text{SED}}$ [ $M_{\odot}\text{yr}^{-1}$ ]	$\text{SFR}_{24}$ [ $M_{\odot}\text{yr}^{-1}$ ]	$\text{SFR}_{\text{H}}$ [ $M_{\odot}\text{yr}^{-1}$ ]	$\text{SFR}_{\text{radio}}$ [ $M_{\odot}\text{yr}^{-1}$ ]	$\log(L_{\text{IR,H}})$ $\log[L_{\odot}]$	$\log(\text{sSFR}_{\text{H}})$ $\log[\text{yr}^{-1}]$	$q_{24}$
$\log(M_{\star}/M_{\odot}) = 11 - 12.2$ (median = 11.1)																
0.1 – 0.5	0.4	229	32.3 $\pm$ 1.5	0.4 $\pm$ 0.3	0.3 $\pm$ 0.7	0.4 $\pm$ 0.5	0.0 $\pm$ 0.7	-0.1 $\pm$ 0.9	5.2 $\pm$ 1.3	0.03	0.4 $\pm$ 0.2	<0.2	1.2 $\pm$ 0.2	<9.2	< -11.9	0.8
0.5 – 1.0	0.8	1222	21.3 $\pm$ 0.8	0.0 $\pm$ 0.1	0.2 $\pm$ 0.3	-0.2 $\pm$ 0.2	-0.2 $\pm$ 0.3	-0.1 $\pm$ 0.4	5.2 $\pm$ 0.5	0.13	1.6 $\pm$ 0.5	<0.3	6.2 $\pm$ 0.6	<9.5	< -11.7	0.6
1.0 – 1.5	1.2	733	15.9 $\pm$ 0.9	0.1 $\pm$ 0.2	-0.2 $\pm$ 0.4	-0.2 $\pm$ 0.3	0.2 $\pm$ 0.4	0.4 $\pm$ 0.5	3.6 $\pm$ 0.6	0.42	3.3 $\pm$ 1.1	<0.8	11.1 $\pm$ 2.0	<9.9	< -11.2	0.6
1.5 – 2.0	1.7	288	8.8 $\pm$ 1.1	-0.4 $\pm$ 0.3	-0.4 $\pm$ 0.6	-0.8 $\pm$ 0.5	-0.7 $\pm$ 0.6	-0.1 $\pm$ 0.8	2.3 $\pm$ 0.9	0.35	3.0 $\pm$ 1.1	<2.9	16.3 $\pm$ 6.6	<10.4	< -10.7	0.6
2.0 – 2.5	2.2	174	13.4 $\pm$ 1.5	-0.4 $\pm$ 0.4	0.5 $\pm$ 0.8	-0.4 $\pm$ 0.6	-0.1 $\pm$ 0.8	0.3 $\pm$ 1.0	4.2 $\pm$ 1.2	0.71	6.9 $\pm$ 2.5	<7.1	59.6 $\pm$ 17.4	<10.8	< -10.3	0.5
2.5 – 3.0	2.6	65	10.8 $\pm$ 2.2	-0.4 $\pm$ 0.6	0.1 $\pm$ 1.3	-0.6 $\pm$ 1.0	-0.1 $\pm$ 1.4	-0.0 $\pm$ 1.6	6.5 $\pm$ 2.2	1.20	11.4 $\pm$ 4.8	<17.6	145.0 $\pm$ 49.2	<11.2	< -9.9	0.2
$\log(M_{\star}/M_{\odot}) = 10.6 - 11.0$ (median = 10.8)																
0.1 – 0.5	0.4	502	25.2 $\pm$ 1.0	0.6 $\pm$ 0.2	1.0 $\pm$ 0.5	0.0 $\pm$ 0.4	-0.7 $\pm$ 0.5	-0.6 $\pm$ 0.6	3.5 $\pm$ 0.8	0.02	0.3 $\pm$ 0.1	<0.1	0.8 $\pm$ 0.1	<9.0	< -11.8	0.9
0.5 – 1.0	0.8	2167	14.2 $\pm$ 0.6	0.0 $\pm$ 0.1	-0.0 $\pm$ 0.2	-0.7 $\pm$ 0.2	-0.6 $\pm$ 0.2	-0.2 $\pm$ 0.3	1.7 $\pm$ 0.4	0.10	1.0 $\pm$ 0.3	<0.2	2.0 $\pm$ 0.3	<9.3	< -11.4	0.9
1.0 – 1.5	1.2	1646	8.4 $\pm$ 0.5	-0.1 $\pm$ 0.1	-0.4 $\pm$ 0.3	-1.1 $\pm$ 0.2	-1.1 $\pm$ 0.3	-0.8 $\pm$ 0.3	1.6 $\pm$ 0.4	0.23	1.5 $\pm$ 0.5	<0.5	4.8 $\pm$ 1.2	<9.7	< -11.0	0.7
1.5 – 2.0	1.7	516	6.0 $\pm$ 0.8	-0.2 $\pm$ 0.2	-0.3 $\pm$ 0.5	-1.5 $\pm$ 0.3	-1.5 $\pm$ 0.5	-0.9 $\pm$ 0.6	2.1 $\pm$ 0.7	0.30	1.9 $\pm$ 0.7	<2.2	15.3 $\pm$ 5.1	<10.3	< -10.4	0.5
2.0 – 2.5	2.2	295	8.5 $\pm$ 1.2	-0.2 $\pm$ 0.3	0.2 $\pm$ 0.6	-0.9 $\pm$ 0.5	-0.6 $\pm$ 0.6	-0.4 $\pm$ 0.8	2.3 $\pm$ 1.0	0.65	4.6 $\pm$ 1.7	<5.9	36.0 $\pm$ 14.8	<10.8	< -10.0	0.6
$\log(M_{\star}/M_{\odot}) = 10.2 - 10.6$ (median = 10.4)																
0.1 – 0.5	0.4	699	12.8 $\pm$ 0.8	0.5 $\pm$ 0.2	1.0 $\pm$ 0.4	-0.9 $\pm$ 0.3	-1.5 $\pm$ 0.4	-1.2 $\pm$ 0.5	2.6 $\pm$ 0.7	0.01	0.1 $\pm$ 0.1	<0.1	0.6 $\pm$ 0.1	<8.9	< -11.4	0.7
0.5 – 1.0	0.8	2281	10.1 $\pm$ 0.5	0.1 $\pm$ 0.1	-0.1 $\pm$ 0.2	-1.0 $\pm$ 0.2	-1.2 $\pm$ 0.2	-0.8 $\pm$ 0.3	0.9 $\pm$ 0.3	0.06	0.7 $\pm$ 0.2	<0.2	1.2 $\pm$ 0.3	<9.3	< -11.1	1.1
1.0 – 1.5	1.2	1199	5.4 $\pm$ 0.6	-0.1 $\pm$ 0.1	0.0 $\pm$ 0.3	-1.4 $\pm$ 0.2	-1.2 $\pm$ 0.3	-0.7 $\pm$ 0.4	1.3 $\pm$ 0.5	0.15	0.9 $\pm$ 0.3	<0.6	4.0 $\pm$ 1.4	<9.8	< -10.6	0.6
1.5 – 2.0	1.7	432	5.4 $\pm$ 1.0	-0.2 $\pm$ 0.2	0.1 $\pm$ 0.5	-1.4 $\pm$ 0.4	-1.3 $\pm$ 0.5	-0.8 $\pm$ 0.6	2.2 $\pm$ 0.8	0.31	1.7 $\pm$ 0.7	<2.4	16.2 $\pm$ 5.6	<10.4	< -10.0	0.4
$\log(M_{\star}/M_{\odot}) = 9.8 - 10.2$ (median = 10.0)																
0.1 – 0.5	0.4	583	13.1 $\pm$ 0.8	0.3 $\pm$ 0.2	0.1 $\pm$ 0.4	-1.8 $\pm$ 0.3	-2.1 $\pm$ 0.5	-1.9 $\pm$ 0.5	1.8 $\pm$ 0.7	0.01	0.1 $\pm$ 0.1	<0.1	0.5 $\pm$ 0.1	<8.9	< -11.0	0.9
0.5 – 1.0	0.8	1303	6.4 $\pm$ 0.6	-0.1 $\pm$ 0.1	-0.1 $\pm$ 0.3	-1.2 $\pm$ 0.2	-1.3 $\pm$ 0.3	-0.7 $\pm$ 0.4	0.8 $\pm$ 0.4	0.06	0.4 $\pm$ 0.1	<0.3	1.1 $\pm$ 0.4	<9.4	< -10.6	0.9
1.0 – 1.5	1.2	673	4.5 $\pm$ 0.7	0.1 $\pm$ 0.2	-0.4 $\pm$ 0.4	-1.3 $\pm$ 0.3	-1.3 $\pm$ 0.4	-0.7 $\pm$ 0.5	1.2 $\pm$ 0.6	0.21	0.7 $\pm$ 0.3	<0.8	3.6 $\pm$ 1.8	<9.9	< -10.1	0.6

NOTE. — The median redshifts ( $\overline{z_{\text{phot}}}$ ), the number of QGs stacked ( $N_{\text{stack}}$ ), and the stacked flux densities are listed.  $\text{SFR}_{\text{SED}}$  is the median SFR from the UV-to-IRAC SED fitting. We infer SFRs from the stacked flux densities (Section 4.2), assuming that the 24  $\mu\text{m}$  and radio emissions originate from SF only. The IR luminosity and specific SFR upper limits ( $L_{\text{IR,H}}$  and  $\text{sSFR}_{\text{H}}$ ) inferred from the *Herschel* upper limits are shown in logarithmic units. The radio index  $q_{24}$  is computed as  $\log(S_{24\mu\text{m}}/S_{\text{radio}})$ .